materials

MDPI

Communication

Low-Temperature Synthesis of Bi_2S_3 Hierarchical Microstructures via Co-Precipitation and Digestive Process in Aqueous Medium

José Alfonso Carrasco-González [1,2], Rebeca Ortega-Amaya [3], Esteban Díaz-Torres [1], Manuel A. Pérez-Guzmán [4,*] and Mauricio Ortega-López [2,*]

1 Sección de Electrónica del Estado Sólido, Departamento de Ingeniería Eléctrica, Centro de Investigación y de Estudios Avanzados del Instituto Politécnico Nacional, Av. IPN No. 2508, Ciudad de México 07360, Mexico; jose.carrasco@cinvestav.mx (J.A.C.-G.); ediaz@cinvestav.mx (E.D.-T.)

2 Programa de Doctorado Transdisciplinario en Desarrollo Científico y Tecnológico para la Sociedad, Centro de Investigación y de Estudios Avanzados del Instituto Politécnico Nacional, Av. IPN No. 2508, Ciudad de México 07360, Mexico

3 CICFIM-Facultad de Ciencias Físico Matemáticas, Universidad Autónoma de Nuevo León, Av. Universidad S/N, Cuidad Universitaria, San Nicolás de los Garza, Nuevo León 66451, Mexico; orebeca@ymail.com

4 Departamento de Física, Universidad Autónoma Metropolitana-Iztapalapa, Av. San Rafael Atlixco No. 186, Ciudad de México 09340, Mexico

* Correspondence: pgalejandro@yahoo.com (M.A.P.-G.); ortegal@cinvestav.mx (M.O.-L.); Tel.: +52-55-5804-4615 (M.A.P.-G.); +52-55-5747-3800 (ext. 6260) (M.O.-L.)

Abstract: Bismuth sulfide (Bi_2S_3) nanostructures have gained significant attention in the fields of catalysis, optoelectronics, and biomedicine due to their unique physicochemical properties. This paper introduces a simple and cost-effective method for producing Bi_2S_3 microstructures at low temperatures (25 and 70 °C). These microstructures are formed by the hierarchical self-assembly of Bi_2S_3 nanoparticles, which are typically 15–40 nm in size. The nanoparticles are synthesized by the co-precipitation of thioglycolic acid, thioacetamide, and bismuth nitrate in water. The study delves into the phase composition and morphological evolution of the microstructures, concerning the chemical composition of the solution and the synthesis temperature. X-ray analysis has confirmed the formation of single-phase bismuthinite Bi_2S_3. The synthesis process generates primary building blocks in the form of 15–40 nm Bi_2S_3 nanocrystals, which then go through a hierarchical self-assembly process to produce a range of micrometer-sized structures. A scanning electron microscopy examination revealed that the primary nanoparticles self-assemble into quasi-1D worm-like nanostructures, which then self-assemble to create sponge-shaped microstructures. These structures subsequently self-organize and refine into either flower- or dandelion-like microstructures, mostly depending on the synthesis temperature and the chemistry of the digestion medium.

Keywords: Bi_2S_3; co-precipitation; hierarchical self-assembly; microstructure

Citation: Carrasco-González, J.A.; Ortega-Amaya, R.; Díaz-Torres, E.; Pérez-Guzmán, M.A.; Ortega-López, M. Low-Temperature Synthesis of Bi_2S_3 Hierarchical Microstructures via Co-Precipitation and Digestive Process in Aqueous Medium. *Materials* **2024**, *17*, 1818. https://doi.org/10.3390/ma17081818

Academic Editor: Mariana Prodana

Received: 4 March 2024
Revised: 4 April 2024
Accepted: 10 April 2024
Published: 16 April 2024

1. Introduction

The development of advanced materials with unique properties holds immense potential for various technological and scientific applications. Amongst these, 3D hierarchical nanostructures of binary V-VI compounds have gained significant attention due to their exceptional structural architecture and enhanced performance in energy conversion-related and environmental remediation applications [1]. Therefore, it is crucial to establish cost-effective and straightforward processes for synthesizing these materials. In this regard, colloidal chemistry in an aqueous medium can play a pivotal role in achieving this objective.

The semiconductor material bismuth sulfide (Bi_2S_3) has raised special interest due to its optical and electrical properties, which can be widely tailored by controlling the size and shape of its morphological features during synthesis [2–6]. Crystalline Bi_2S_3 exhibits

n-type conductivity and has a direct band with a band gap energy of E_g = 1.4 eV. However, various synthesis methods for Bi_2S_3 nanocrystals reported E_g values ranging from 1.3 to 1.7 eV [6,7]. In comparison to other highly toxic mineral sulfides such as Greenockite (CdS), Orpiment (As_2S_3), or Cinnabar (HgS), Bismutinite (Bi_2S_3) can be considered a compound with low or no toxicity [8–11].

Bismuth sulfide exhibits a unique crystal structure, characterized by a unit cell that belongs to the orthorhombic crystalline system Pnma. The lattice parameters for Bi_2S_3 are a = 11.15 Å, b = 11.30 Å, and c = 3.981 Å. Within its unit cell, there are 20 atoms, which consist of four Bi_2S_3 units. These atoms arrange themselves in slats along the c-axis and are stacked together by intermolecular bonds along the a-axis, resulting in the formation of three-dimensional lamella-like structures [12]. These structural properties allow Bi_2S_3 to develop crystalline habits such as nanorods, nanosheets, and acicular structures [13–21].

Recently, nanostructured Bi_2S_3 has attracted significant attention due to its ease of preparation using various techniques. Chemical methods where a powdered material [22], thin films [23], and solutions [24] were obtained and physical methods that resulted in films and bulk materials [25–27] were proven. Consequently, this has allowed extensive bismuth sulfide study of its potential applications in polymer/Bi_2S_3 hybrid solar cells, hydrogen storage [28,29], and thin films for electronic devices [30–32].

The primary aim of this study is to synthesize nanostructures of Bi_2S_3 utilizing a cost-effective and straightforward process, such as co-precipitation in an aqueous medium.

2. Experimental Procedures

2.1. Reagents and Material Synthesis

The Bi_2S_3 nanostructures were prepared by co-precipitation using aqueous solutions of bismuth nitrate pentahydrate ($Bi(NO_3)_3 \bullet 5H_2O$, ≥98% Sigma-Aldric, Toluca, Mexico), thioglycolic acid (TGA, $HSCH_2CO_2H$, ≥98% Sigma-Aldrich), and thioacetamide (TAA, $H_2C{=}CSNH_2$, Analytyka, Nuevo Leon, Mexico). All reagents are used without any additional purification process.

In all experiments, the precursor solutions of sulfur and bismuth ions were separately prepared as follows:

Solution A. The TAA solution was prepared at room temperature by dissolving 451 mg of TAA in 60 mL of deionized water for 3 min, with the concentration being 0.1 M in TAA.

Solution B: The bismuth nitrate solution involved the direct dissolution of the bismuth salt in TGA within a ball flask with constant magnetic stirring. After complete dissolution (~7 min), 5 mL of deionized water was added, and it was either heated up to 70 °C or maintained at 25 °C for 15 min. Subsequently, 30 mL of solution A was mixed with 30 mL of deionized water. The resulting solution was completely mixed with solution B. This mixing triggered a rapid reaction, causing the solution color to change from yellow to orange, then red, and finally a dark brown. The colloidal reaction was allowed to proceed for 60 min at the chosen synthesis temperature. The minimum reported reaction time is that measured just after the mixing process was performed, being around 3 min.

Following the synthesis process, the heating source was turned off, and the resulting solution was left to undergo a 24 h digestion period. This digestion process facilitates the separation of the solid phase, forming a sedimented floc, from the liquid phase. The liquid phase, containing dispersed Bi_2S_3 nanoparticles and byproducts, was carefully poured off. To ensure a neutral pH, the floc was subjected to multiple washes. Finally, the floc was effectively dried by heating it at 70 °C. Figure 1 details the entire Bi_2S_3 synthesis process described in this section.

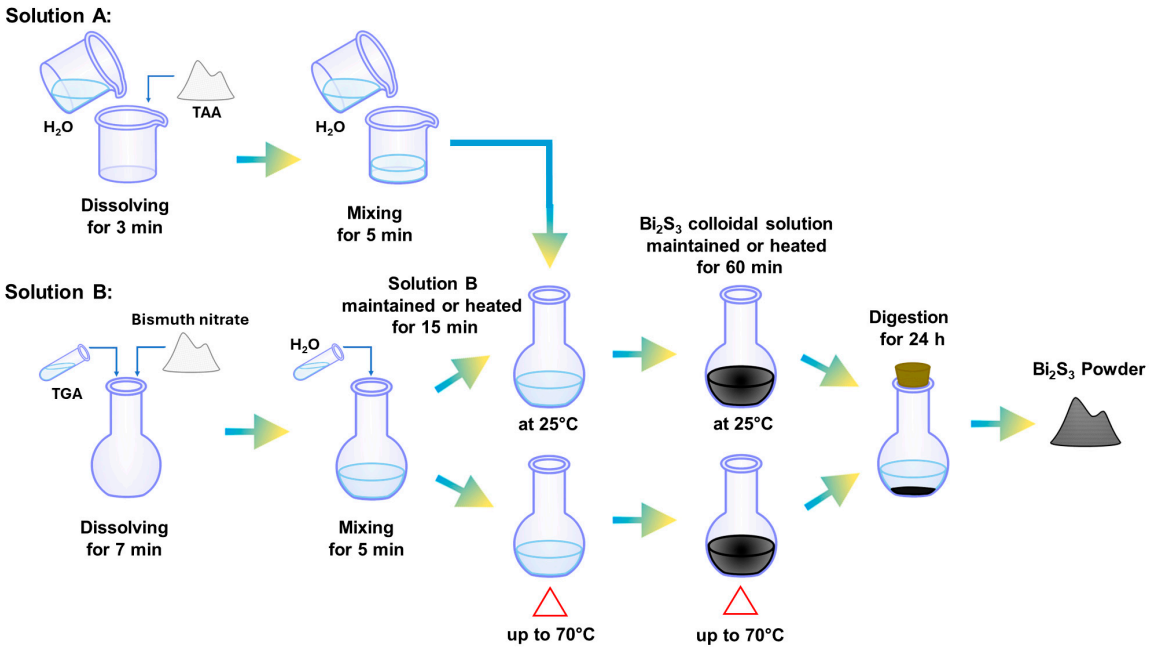

Figure 1. Schematic representation of Bi_2S_3 colloidal synthesis process, indicating the dissolving, mixing, reaction, digestion, and powder obtention stages.

Four series of experiments were prepared and labeled as BiS10X, BiS20X, and BiS30X (X = 1–3), where the TAA concentration, the TGA one, and the $Bi(NO_3)_3 \bullet 5H_2O$ one were varied, respectively, and the BiSTAX series, where the reaction was performed at 25 °C, varying the TGA concentration. However, while some experiments produced samples with similar structural and morphological features, the most notable distinction was observed in samples prepared at varying temperatures. For the purpose of our discussion, we have selected samples prepared at 25 and 70 °C as representative examples.

2.2. Characterization Techniques

The phase composition of Bi_2S_3 nanostructures was assessed by X-ray diffraction (XRD), and a PANalytical X'Pert-PRO diffractometer (Malvern Panalytical, Malvern, UK) with Cu-Kα emission was used for this purpose. The scan range was set from 15° to 70° with a step size of 0.04°. The crystal size was determined by analyzing the position of the highest intensity peaks and their corresponding Full Width at Half Maximum (FWHM) using the Sherrer equation, with a value of $k = 0.9$ [33]. The morphological characterization of the powders was carried out using scanning electron microscopy (SEM), where a FE-SEM Zeiss Auriga (Carl Zeiss Microscopy GmbH, Jena, Germany) operating at 5 and 10 kV was utilized for this analysis.

3. Results and Discussion

The phase composition and morphology of the Bi_2S_3 powder were analyzed by XRD and SEM, respectively. As stated above, various experimental conditions led to samples with similar compositions and morphological developments. The following discussion is based on the representative samples synthesized at room temperature (~25 °C, BiSTAX) and 70 °C (BiS10X).

3.1. XRD Analysis

The diffractograms shown in Figure 2 correspond to the Bi_2S_3 samples corresponding to the BiSTAX series (Figure 2a) and BiS10X series (Figure 2b). It is worth noting that well-crystallized samples were obtained, despite being prepared at low temperature (25 °C). All the observed diffraction lines are attributed to the orthorhombic phase of Bi_2S_3 bismuthinite, according to the ICCD No. 00-006-0333 reference card. No diffraction peaks corresponding

to solid phases other than bismuthinite Bi_2S_3 were detected. As previously mentioned, the Bi salt was directly mixed with the TGA to minimize Bi-ion hydrolysis and the subsequent formation of complex hydrated bismuth oxide species [29]. This is because both thioglycolic acid and thioacetamide serve a dual role as Bi-ion ligands and as a source of sulfur (S) [30,31]. This successful process of preparing the precursor solution effectively prevents the formation of impurity phases other than Bi_2S_3.

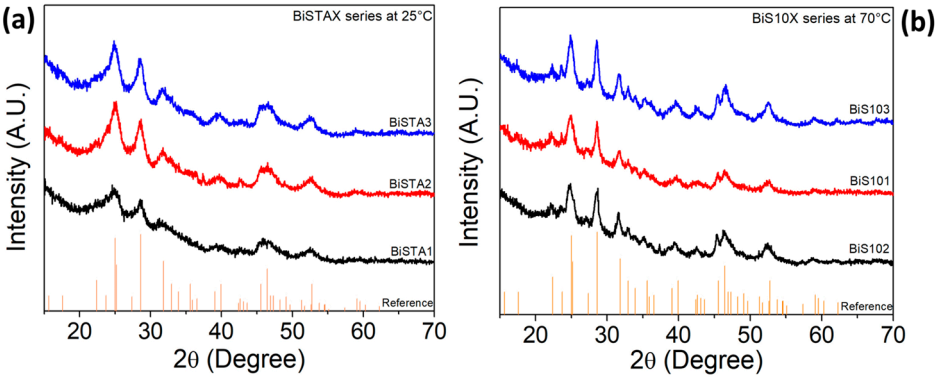

Figure 2. XRD patterns of the Bi_2S_3 samples. (**a**) Samples corresponding to the BiSTAX series (synthesized at 25 °C) and (**b**) samples corresponding to the BiS10X series (synthesized at 70 °C). Notice that the vertical lines belonging to the bismuthinite mineral reference card ICCD No. 00-006-0333 were added.

The lattice parameters were estimated using the XRD data from the most intense peaks, resulting around a = 11.18 Å, b = 11.43 Å, and c = 3.98 Å. These values slightly differ from those reported in the ICCD reference card. That is, a and b are larger than the reference values in about 0.27 and 1.15%, respectively, indicating a tensile stress; on the contrary, the lattice parameter c resulted in a minimum compression stress of 0.03%, which represents a practically negligible difference. The crystallite size, on the other hand, was found to vary in the 15–40 nm range. Nevertheless, as discussed below, in some cases, certain experimental parameters slightly affected the final morphology of the self-assembled microstructures.

3.2. Morphological Analysis

The morphology of the Bi_2S_3 powder was analyzed using SEM. Figure 3 presents SEM images of representative samples prepared at room temperature (25 °C) (Figure 3a) and 70 °C (Figure 3b). The synthesis procedure, which combines co-precipitation and digestion, resulted in Bi_2S_3 microstructures with a wide variety of forms, all seemingly derived from a self-assembly process. The XRD analysis confirmed that these microstructures are composed of 15–40 nm-in-size Bi_2S_3 nanoparticles, whereas the SEM images revealed larger Bi_2S_3 structures in the micrometer range. Therefore, the SEM characterization suggests that the synthesis procedure produces nanosized Bi_2S_3 as the primary building blocks, from which microstructures develop through sequential self-assembly steps. The dominant morphologies that emerged at different temperatures are highlighted in Figure 3. At room temperature, Figure 3a,c show the formation of sponge-, urchin-, and dandelion-like bismuth sulfide microstructures, which were influenced by the TGA content. On the other hand, at 70 °C (Figure 3b,d), sponge-, urchin, flower- and coral-like microstructures are predominantly observed under all the tested experimental conditions. Detailed close-up views of each morphology can be seen in Figure 3c,d. The sponge-like and dandelion structures have average sizes of 1.16 μm and 0.90 μm, respectively, while the flower-like structure is 1.30 μm in size, and the maximal visible cross-sectional length of their leaves is 122.73 nm.

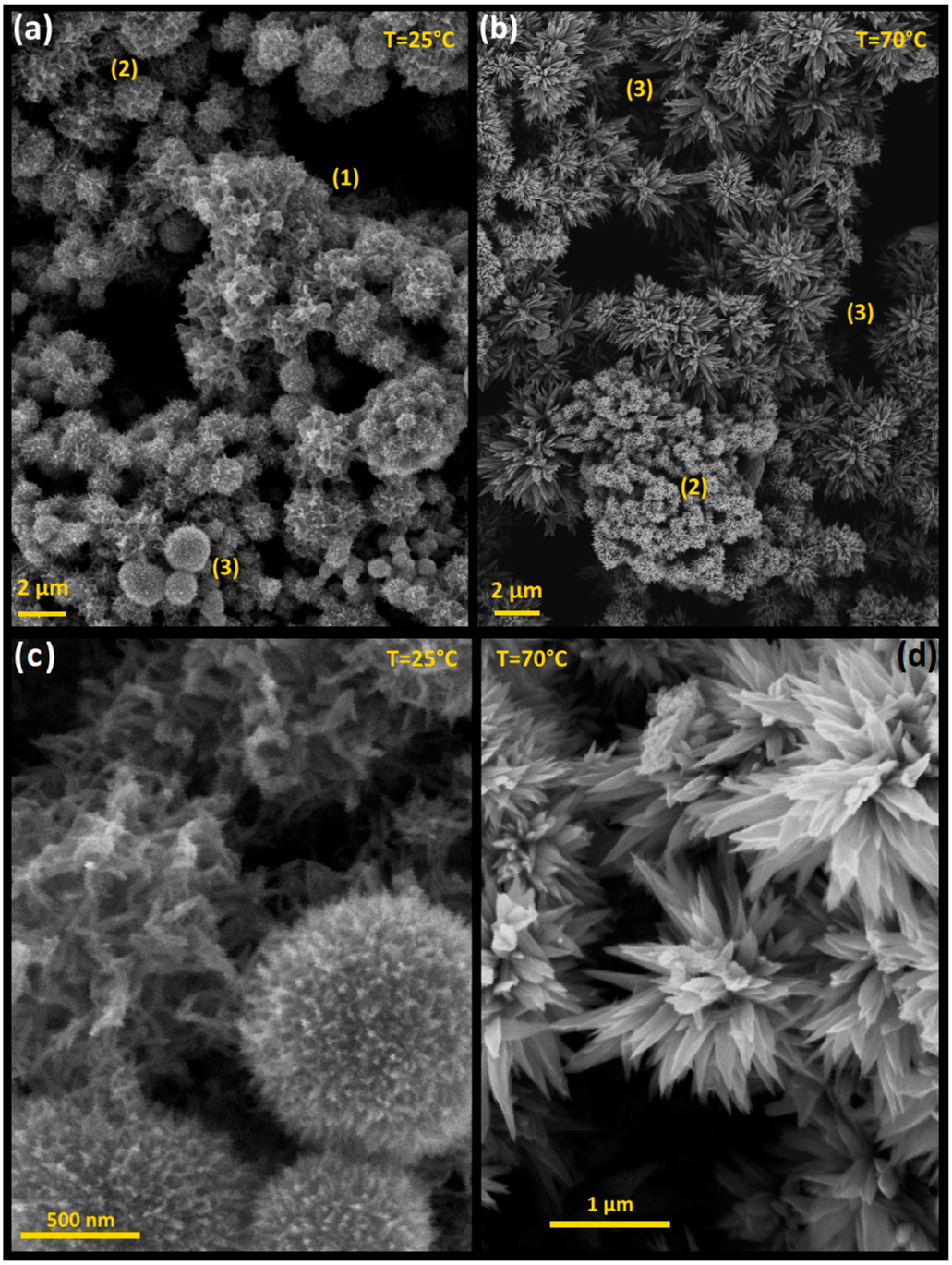

Figure 3. (**a**,**b**) Panoramic SEM images of the two Bi_2S_3 crystalline acicular structures, simultaneously displaying different self-assembly stages. (1) indicates the early stage (worm formation), (2) sponge-like formation stage, and (3) formed acicular structures (dandelions at 25 °C or flowers at 70 °C). (**c**,**d**) Close-up view of dandelion and flower Bi_2S_3 crystalline microstructures.

To gain a better understanding of the sequential self-assembly process, aliquots from representative precipitation reactions were taken out ~1 min after starting the precipitation reaction. Figure 4a illustrates the morphological evolution of Bi_2S_3 microstructures after ~1 min of initiating phase solid precipitation at 70 °C. It is evident that upon the onset of precipitation, nanoscale Bi_2S_3 particles undergo self-assembly to form worm-like nanostructures, which then further assemble into intricate sponge-like microstructures, indicating that the hierarchical self-assembly of Bi_2S_3 nanoparticles begins accompanying the solid phase precipitation and continues to progress during the digestive process, as shown in

Figure 3b. Figure 4a reveals that worm-like structures are commonly observed in samples synthesized at both 25 °C and 70 °C and that they self-assemble into a woven network sponge-like microstructure, as shown in Figure 4b.

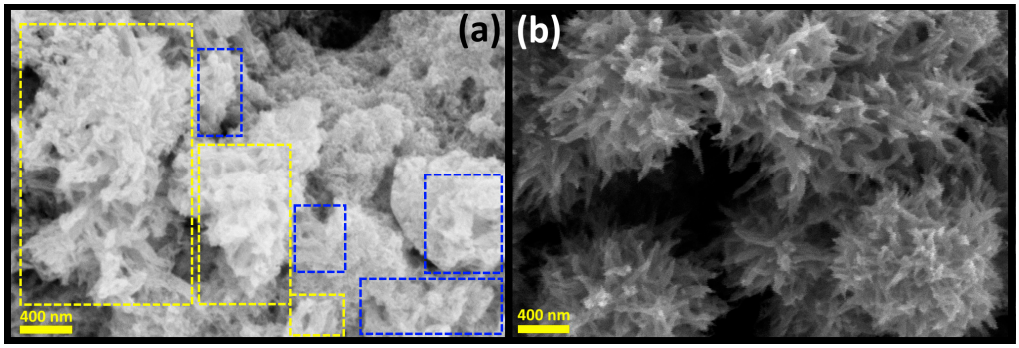

Figure 4. SEM images of Bi_2S_3 crystals in some stages of the self-assembly process. (**a**) Rolled-up worm formation and (**b**) sponge-like structure formation stage. Rectangles were added to the image (**a**) to indicate the unrolled (blue) and rolled-up worm (yellow) crystalline structures.

We have proposed a potential pathway that leads to the formation of microstructures by closely examining the SEM images shown in Figure 3a,b. We have assumed that these figures serve to illustrate the critical steps of the self-assembly process. That is, we propose that the SEM images include micron-sized Bi_2S_3 with different degrees of development. The different stages of self-assembly and formation are highlighted in Figure 3a,b, denoted by numbers, illustrating (1) the early stage of worm formation, (2) the sponge-like formation stage, and (3) the final stage of acicular microstructure formation. Based on Figure 3a, we propose that the morphology progresses sequentially as follows:

Initially, primary Bi_2S_3 nanoparticles self-assemble into worm-like 1D nanostructures, which subsequently group and coalesce into waved worm-like structures resembling sponge-like microstructures. The subsequent shape modification of self-assembled Bi_2S_3 microstructures develops during the digestion process. Figure 4a illustrates the morphological details of the Bi_2S_3 microstructures. It is evident that at the early stage of the self-assembly process, worm- and sponge-like microstructures emerged as the dominant ones. These develop into porous Bi_2S_3 microstructures resembling a sponge-like structure, which are prone to further shape transformations during the digestion process, depending on the temperature. The worm-like and sponge-shaped structures appear to be a common occurrence across all the samples, regardless of the experimental conditions used for their preparation. This assertion is illustrated by Figure 4b for synthesis at room temperature.

Following this starting formation, the sponge-shaped microstructures are subjected to Ostwald ripening, redissolution, and reshaping during digestion to achieve their final shape. At 25 °C, the mechanisms responsible for consolidating and refining the crystalline microstructure typically result in mostly porous, dandelion-like Bi_2S_3 structures, as seen in Figure 3a,c. Conversely, the samples prepared at 70 °C exhibit a transformation from nanoworms into acicular structures, which then self-assemble to form flower-like microstructures, as shown in Figure 3b,d.

Figure 5 provides a summary of the self-assembly and digestion processes described above.

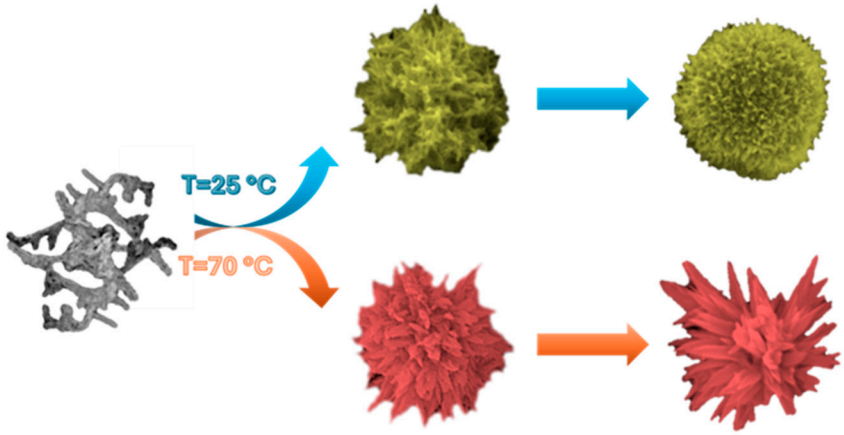

Figure 5. Schematic representation of the hierarchical self-assembly process of Bi_2S_3 crystals changing into sponge-like and acicular structures.

To compare our results with other related works, it is worth mentioning that the synthesis of bismuth sulfide microstructures has extensively been studied, and Bi_2S_3 microstructures like those reported here have been observed using both chemical and physical synthesis. For instance, urchin-like Bi_2S_3 nanocrystals were obtained by Ma, Li, Chen, Sasikala, and Sang [21,22,34–36] by chemical techniques, and Song, Ten Haaf, and Li [25,37,38] obtained needle-, block-, bar-, and rod-shaped ones by vacuum techniques. Salavati-Niasari and Zhang et al. [20,39] synthesized urchin- and dandelion-like microstructures by using aqueous chemical methods containing TGA and/or thioacetamide. These researchers conducted a comprehensive analysis to propose that the TGA plays a crucial role in the development of such Bi_2S_3 microstructures.

The observations above indicate that the morphological development of nanostructured Bi_2S_3 appears to be unaffected by the synthesis method and is primarily determined by the crystal structure of Bi_2S_3.

Our results significantly differ from others previously reported. In our study, nanosized Bi_2S_3 particles self-assembled into worm-like nanostructures almost at the onset of precipitation. Subsequently, the self-assembly steps of these 1D nanostructures produced sponge-, urchin-, dandelion-, or flower-like Bi_2S_3 microstructures. The dandelion formation was favored when the synthesis was carried out at room temperature, regardless of the TGA content. Whereas, for the synthesis at 70 °C, all the prepared samples exhibited a similar morphology as that developed by the BiS10X series, resembling a flower-like structure. On the basis of these observations, the hierarchical self-assembly pathway leading to the formation of bismuth sulfide microstructures is primarily dictated by the crystalline structure of Bi_2S_3 and by the chemistry of the solution in which the digestion process takes place. Notice that digestion was carried out at room temperature.

In our experiments, the role of TGA as an assembly director agent was not clear enough. In this sense, our interpretation differs from that of Salavati et al. [16], who proposed that TGA directs the final microstructure shape of Bi_2S_3. Instead, our results suggest that the crystal habit of Bi_2S_3, the synthesis temperature, and the solution digestion are the key factors influencing the microstructure formation. By understanding these factors, we can gain valuable insights into the synthesis of bismuth sulfide microstructures and potentially control their shape and properties.

Overall, this research demonstrates the fascinating hierarchical self-assembly process that leads to the formation of a great variety of Bi_2S_3 microstructures using simple and cheap synthesis techniques. The study also highlights the impact of digestion on the refinement of these structures, providing valuable insights into their formation and development. The SEM analysis has provided valuable information related to the potential applications of Bi_2S_3 in various fields such as optoelectronics, catalysis, and energy storage. The thorough investigation of the morphology of Bi_2S_3 powders by SEM has enhanced our

understanding of their physical properties and paved the way for their utilization in advanced device research.

4. Conclusions

In conclusion, this study introduces a simple and cost-effective method for producing Bi_2S_3 microstructures in a variety of sizes and shapes. The synthesis process involves co-precipitation at low temperatures (25 and 70 °C), followed by a 24 h digestion period. This method results in a highly pure Bi_2S_3 powder. The unique morphology of the Bi_2S_3 microstructures is achieved through a hierarchical self-assembly process and a digestion mechanism.

Starting with Bi_2S_3 particles ranging from 15 to 40 nm in size, it was observed that these nanoparticles self-assemble into worm-like 1D nanostructures during the precipitation reaction. These nanoworms then further assemble into sponge-, urchin-, and dandelion or flower-like Bi_2S_3 microstructures. What sets our results apart from previous studies is the role of worm-like nanostructures as building blocks for more complex forms. These structures undergo shape transformations due to Ostwald ripening, nanocrystal adhesion, and reshaping during the digestion process.

The final shape of the Bi_2S_3 microstructures, particularly the crystal habit of Bi_2S_3, is influenced by the chemical composition of the solution and temperature. Dandelion-like and flower-like microstructures were observed at 25 and 70 °C, respectively. The resulting Bi2S3 microstructures morphology have a high surface area, making them ideal for applications in sensing and catalysis.

Author Contributions: J.A.C.-G. participated in the investigation, methodology, conceptualization, and writing original draft of this manuscript, R.O.-A. and E.D.-T. participated in the methodology, validation, writing original draft, review, and editing, M.A.P.-G. and M.O.-L. participated in the conceptualization, supervision, writing original draft, review, and editing. All authors have read and agreed to the published version of the manuscript.

Funding: This research received no external funding.

Data Availability Statement: Data are contained within the article.

Acknowledgments: The authors wish to thank Álvaro Guzmán Campuzano for assistance in the material synthesis, Adolfo Tavira Fuentes for the XRD measurements, and LANE CINVESTAV-IPN for the SEM images, and CONAHCYT-México for the postdoctoral fellowships provided to R.O.-A., E.D.-T. and M.A.P.-G.

Conflicts of Interest: The authors declare no conflicts of interest.

References

1. Boles, M.A.; Engel, M.; Talapin, D.V. Self-assembly of colloidal nanocrystals: From intricate structures to functional materials. *Chem. Rev.* **2016**, *116*, 11220–11289. [CrossRef] [PubMed]
2. Miller, N.C.; Bernechea, M. Research Update: Bismuth based materials for photovoltaics. *APL Mater.* **2018**, *6*, 084503. [CrossRef]
3. Aresti, M.; Saba, M.; Piras, R.; Marongiu, D.; Mula, G.; Quochi, F.; Mura, A.; Cannas, C.; Mureddu, M.; Ardu, A.; et al. Colloidal Bi_2S_3 nanocrystals: Quantum size effects and midgap states. *Adv. Funct. Mater.* **2014**, *24*, 3341–3350. [CrossRef]
4. Ma, J.; Yang, J.; Jiao, L.; Wang, T.; Lian, J.; Duan, X.; Zheng, W. Bi_2S_3 nanomaterials: Morphology manipulation and related properties. *Dalton Trans.* **2011**, *40*, 10100–10109. [CrossRef] [PubMed]
5. Bernechea, M.; Cao, Y.; Konstantatos, G. Size and bandgap tunability in Bi_2S_3 colloidal nanocrystals and its effect in solution processed solar cells. *J. Mater. Chem. A* **2015**, *3*, 20642–20648. [CrossRef]
6. Calzia, V.; Malloci, G.; Bongiovanni, G.; Mattoni, A. Electronic Properties and Quantum Confinement in Bi_2S_3 Ribbon-like Nanostructures. *J. Phys. Chem. C* **2013**, *117*, 21923–21929. [CrossRef]
7. Rincón, M.E.; Sánchez, M.; George, P.J.; Sánchez, A.; Nair, P.K. Comparison of the Properties of Bismuth Sulfide Thin Films Prepared by Thermal Evaporation and Chemical Bath Deposition. *J. Solid State Chem.* **1998**, *136*, 167–174. [CrossRef]
8. Khan, Z.; Elahi, A.; Bukhari, D.A.; Rehman, A. Cadmium sources, toxicity, resistance and removal by microorganisms-A potential strategy for cadmium eradication. *J. Saudi Chem. Soc.* **2022**, *26*, 101569. [CrossRef]
9. Min, X.; Xu, Q.; Ke, Y.; Xu, H.; Yao, L.; Wang, J.; Ren, H.; Li, T.; Lin, Z. Transformation behavior of the morphology, structure and toxicity of amorphous As_2S_3 during hydrothermal process. *Hydrometallurgy* **2021**, *200*, 105549. [CrossRef]

10. Nádudvari, Á.; Cabała, J.; Marynowski, L.; Jabłońska, M.; Dziurowicz, M.; Malczewski, D.; Kozielska, B.; Siupka, P.; Piotrowska-Seget, Z.; Simoneit, B.R.T.; et al. High concentrations of HgS, MeHg and toxic gas emissions in thermally affected waste dumps from hard coal mining in Poland. *J. Hazard Mater.* **2022**, *431*, 128542. [CrossRef]
11. Guo, J.; Lou, Q.; Qiu, Y.; Wang, Z.Y.; Ge, Z.H.; Feng, J.; He, J. Remarkably enhanced thermoelectric properties of Bi_2S_3 nanocomposites via modulation doping and grain boundary engineering. *Appl. Surf. Sci.* **2020**, *520*, 146341. [CrossRef]
12. Ajiboye, T.O.; Onwudiwe, D.C. Bismuth sulfide based compounds: Properties, synthesis and applications. *Results Chem.* **2021**, *3*, 100151. [CrossRef]
13. Dong, Y.; Hu, M.; Zhang, Z.; Zapien, J.A.; Wang, X.; Lee, J.M. Hierarchical self-assembled Bi_2S_3 hollow nanotubes coated with sulfur-doped amorphous carbon as advanced anode materials for lithium ion batteries. *Nanoscale* **2018**, *10*, 13343–13350. [CrossRef] [PubMed]
14. Arabzadeh, A.; Salimi, A. Facile Synthesis of Ultra-wide Two Dimensional Bi_2S_3 Nanosheets: Characterizations, Properties and Applications in Hydrogen Peroxide Sensing and Hydrogen Storage. *Electroanalysis* **2017**, *29*, 2027–2035. [CrossRef]
15. Sahu, M.; Park, C. A comprehensive review on bismuth-sulfide-based compounds. *Mater. Today Sustain.* **2023**, *23*, 10441. [CrossRef]
16. Chen, Z.; Cao, M. Synthesis, characterization, and hydrophobic properties of Bi_2S_3 hierarchical nanostructures. *Mater. Res. Bull.* **2011**, *46*, 555–562. [CrossRef]
17. Zhu, G.; Liu, P. Low-temperature urea-assisted hydrothermal synthesis of Bi_2S_3 nanostructures with different morphologies. *Cryst. Res. Technol.* **2009**, *44*, 713–720. [CrossRef]
18. Miniach, E.; Zyna Gryglewicz, G. Solvent-controlled morphology of bismuth sulfide for supercapacitor applications. *J. Mater. Sci.* **2018**, *53*, 16511–16523. [CrossRef]
19. Deshpande, M.P.; Sakariya, P.N.; Bhatt, S.V.; Garg, N.; Patel, K.; Chaki, S.H. Characterization of Bi_2S_3 nanorods prepared at room temperature. *Mater. Sci. Semicond. Process.* **2014**, *21*, 180–185. [CrossRef]
20. Salavati-Niasari, M.; Ghanbari, D.; Davar, F. Synthesis of different morphologies of bismuth sulfide nanostructures via hydrothermal process in the presence of thioglycolic acid. *J. Alloys Compd.* **2009**, *488*, 442–447. [CrossRef]
21. Ma, J.; Liu, Z.; Lian, J.; Duan, X.; Kim, T.; Peng, P.; Liu, X.; Chen, Q.; Yao, G.; Zheng, W. Ionic liquids-assisted synthesis and electrochemical properties of Bi_2S_3 nanostructures. *CrystEngComm* **2011**, *13*, 3072–3079. [CrossRef]
22. Li, Y.; Wei, F.; Ma, Y.; Zhang, H.; Gao, Z.; Dai, L.; Qin, G. Selected-control hydrothermal synthesis and photoresponse properties of Bi_2S_3 micro/nanocrystals. *CrystEngComm* **2013**, *15*, 6611. [CrossRef]
23. Carrillo-Castillo, A.; Rivas-Valles, B.G.; Castillo, S.J.; Ramirez, M.M.; Luque-Morales, P.A. New Formulation to Synthetize Semiconductor Bi_2S_3 Thin Films Using Chemical Bath Deposition for Optoelectronic Applications. *Symmetry* **2022**, *14*, 2487. [CrossRef]
24. Han, P.; Mihi, A.; Ferre-borrull, J.; Pallarés, J.; Marsal, L.F. Interplay Between Morphology, Optical Properties, and Electronic Structure of Solution-Processed Bi_2S_3 Colloidal Nanocrystals. *J. Phys. Chem. C* **2015**, *119*, 10693–10699. [CrossRef]
25. Song, H.; Zhan, X.; Li, D.; Zhou, Y.; Yang, B.; Zeng, K.; Zhong, J.; Miao, X.; Tang, J. Rapid thermal evaporation of Bi_2S_3 layer for thin film photovoltaics. *Sol. Energy Mater. Sol. C* **2016**, *146*, 1–7. [CrossRef]
26. Wu, Y.; Lou, Q.; Qiu, Y.; Guo, J.; Mei, Z.Y.; Xu, X.; Feng, J.; He, J.; Ge, Z.H. Highly enhanced thermoelectric properties of nanostructured Bi_2S_3 bulk materials: Via carrier modification and multi-scale phonon scattering. *Inorg. Chem. Front.* **2019**, *6*, 1374–1381. [CrossRef]
27. Liu, W.; Lukas, K.C.; McEnaney, K.; Lee, S.; Zhang, Q.; Opeil, C.P.; Chen, G.; Ren, Z. Studies on the Bi_2Te_3–Bi_2Se_3–Bi_2S_3 system for mid-temperature thermoelectric energy conversion. *Energy Environ. Sci.* **2013**, *6*, 552–560. [CrossRef]
28. Saha, S.K.; Pal, A.J. Schottky diodes between Bi_2S_3 nanorods and metal nanoparticles in a polymer matrix as hybrid bulk-heterojunction solar cells. *J. Appl. Phys.* **2015**, *118*, 014503. [CrossRef]
29. Jin, R.; Li, G.; Xu, Y.; Liu, J.; Chen, G. Uniform Bi_2S_3 nanorods-assembled hollow spheres with excellent electrochemical hydrogen storage abilities. *Int. J. Hydrogen. Energy* **2014**, *39*, 356–365. [CrossRef]
30. Shkir, M. Improved opto-electronic properties of Bi_2S_3 thin films through trivalent atom (Al^{3+}) doping for photodiode applications. *Surf. Interfaces* **2023**, *40*, 103025. [CrossRef]
31. Chitara, B.; Kolli, B.S.C.; Yan, F. Near-Infrared photodetectors based on 2D Bi_2S_3. Chem. *Phys. Lett.* **2022**, *804*, 139876. [CrossRef]
32. Kim, Y.; Jeong, E.; Joe, M.; Lee, C. Synthesis of 2D semiconducting single crystalline Bi_2S_3 for high performance electronics. *Phys. Chem. Chem. Phys.* **2021**, *23*, 26806–26812. [CrossRef] [PubMed]
33. Uddin, I.; Abzal, S.M.; Kalyan, K.; Janga, S.; Rath, A.; Patel, R.; Gupta, D.K.; Ravindran, T.R.; Ateeq, H.; Khan, M.S.; et al. Starch-Assisted Synthesis of Bi_2S_3 Nanoparticles for Enhanced Dielectric and Antibacterial Applications. *ACS Omega* **2022**, *7*, 42438–42445. [CrossRef] [PubMed]
34. Chen, J.; Qin, S.; Song, G.; Xiang, T.; Xin, F.; Yin, X. Shape-controlled solvothermal synthesis of Bi_2S_3 for photocatalytic reduction of CO_2 to methyl formate in methanol. *Dalton Trans.* **2013**, *42*, 15133. [CrossRef] [PubMed]
35. Sasikala, S.; Balakrishnan, M.; Kumar, M.; Chang, J.H.; Manivannan, M.; Thangabalu, S. Effect of sulfur source and temperature on the morphological characteristics and photocatalytic activity of Bi_2S_3 nanostructure synthesized by microwave irradiation technique. *J. Mater. Sci. Mater. Electron.* **2023**, *34*, 997. [CrossRef]
36. Sang, Y.; Dai, G.; Wang, L.; Gao, X.; Fang, C. Hydrothermal Synthesis of Urchin-like Bi_2S_3 Nanostructures for Superior Visible-light-driven Cr(VI) Removal Capacity. *ChemistrySelect* **2018**, *3*, 7123–7128. [CrossRef]

37. ten Haaf, S.; Sträter, H.; Brüggemann, R.; Bauer, G.H.; Felser, C.; Jakob, G. Physical vapor deposition of Bi_2S_3 as absorber material in thin film photovoltaics. *Thin Solid Films* **2013**, *535*, 394–397. [CrossRef]
38. Li, Z.; Zhang, Q.; Dan, M.; Guo, Z.; Zhou, Y. A facile preparation route of Bi_2S_3 nanorod films for photocatalytic H_2 production from H_2S. *Mater. Lett.* **2017**, *201*, 118–121. [CrossRef]
39. Zhang, Z.; Zhou, C.; Lu, H.; Jia, M.; Lai, Y.; Li, J. Facile synthesis of dandelion-like Bi_2S_3 microspheres and their electrochemical properties for lithium-ion batteries. *Mater. Lett.* **2013**, *91*, 100–102. [CrossRef]